Macromolecules

pubs.acs.org/Macromolecules Article

Elucidating the Influence of Side-Chain Circular Distribution on the Crack Onset Strain and Hole Mobility of Near-Amorphous Indacenodithiophene Copolymers

Parker J. W. Sommerville, Yilin Li, Ban Xuan Dong, Yongcao Zhang, Jonathan W. Onorato, Wesley K. Tatum, Alex H. Balzer, Natalie Stingelin, Shrayesh N. Patel, Paul F. Nealey, and Christine K. Luscombe*

Cite This: *Macromolecules* 2020, 53, 7511–7518 Read Online

ACCESS | Metrics & More | Article Recommendations | Supporting Information

ABSTRACT: Poly(indacenodithiophene-benzothiadiazole) has received significant interest because of its exceptional hole mobility despite its near-amorphous thin-film morphology and brittleness at low M_n. In comparison, poly(indacenodithiophene-benzopyrollodione) (PIDTBPD) has a lower hole mobility but is exceptionally ductile at similar M_n. Herein, we synthesize random indacenodithiophene (IDT) copolymers with varying amounts of incorporated benzothiadiazole and benzopyrollodione (BPD), which introduces varied degrees of backbone twist to each respective polymer system. This allows us to elucidate how the BPD monomer introduction leads to conformational and morphological changes that influence the crack onset strain (CoS) and hole mobility of these near-amorphous IDT copolymers and the rates by which each material property responds to sequentially larger BPD incorporation. Results of density functional theory calculations suggest that BPD introduction does not lead to significant differences in backbone linearity between the studied polymers, and grazing incidence wide-angle X-ray scattering demonstrates that the degree of crystallinity within thin films is not significantly altered. It does, however, lead to a more varied circular distribution of the hexadecyl side chains around the polymer backbone. With increasing BPD incorporation, a crossover point between CoS and hole mobility emerges. At this crossover point, a random copolymer with 30% BPD introduction displays increased CoS and an average hole mobility value equal to that of the PIDTBPD system, suggesting that hole mobility is more sensitive to torsion along the polymer backbone, while the response of the CoS is relatively delayed. The data also suggest that the increase in CoS with increasing BPD content does not arise because of differences in rigidity but because the more circular distribution of the side chains makes polymer chains with sufficient BPD content better able to flow.

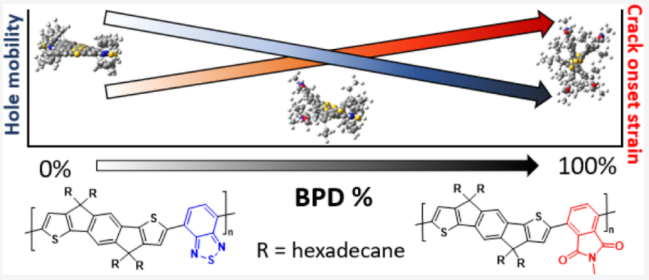

INTRODUCTION

π-Conjugated polymers (CPs) are being investigated as electronic components in a wide range of applications including organic field effect transistors (OFETs)[1] and organic photovoltaics.[2] The motivation for the usage of CPs in electronic devices includes their low mass density, solution processability, and compatibility with high-throughput manufacturing techniques.[3] Moreover, some CPs are suitable materials for use in deformable electronic devices because of their inherent mechanical properties and electronic properties.[4] Initially, it was believed that highly crystalline polymer films would be necessary to achieve efficient charge transport, and a significant effort was made to increase the degree of crystallinity of CP films.[5,6] A more recent understanding has uncovered that a long-range order is not strictly necessary[7] as CPs with low degrees of crystallinity and highly efficient charge transport along planar conjugated backbones have displayed mobilities in excess of 1 $cm^2 V^{-1} s^{-1}$.[8] These CPs fall into the class of near-amorphous CPs, forming only small local aggregates rather than larger crystallites.[9] The existence of local aggregates plays a crucial role in charge transport because they provide the necessary locations where interchain charge transfer can occur.[10] These highly amorphous systems that demonstrate high charge mobility are interesting as they may allow effective strain dissipation.[11,12] Near-amorphous CPs have, thus, the potential to strike a balance between mechanical properties and electronic properties, which makes them target polymers for deformable material applications, including wearable consumer and medical electronics.[13,14]

Received: March 4, 2020
Revised: August 2, 2020
Published: August 18, 2020

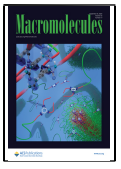

https://dx.doi.org/10.1021/acs.macromol.0c00512
Macromolecules 2020, 53, 7511–7518

To warrant its use in a deformable device, a CP must display effective and robust electrical mobility and be able to withstand mechanical deformation. CP thin films are subjected to stress during deformation. As stress builds, polymer chains will attempt to dissipate stress incrementally by reorganizing into new conformations,[15] often aligning in the direction of strain before undergoing plastic deformation.[11] If the chains are prohibited from reorganizing because of the strength of intermolecular forces between polymer chains, then undissipated stress may be released through more sudden events such as chain pullout,[15] which can induce brittle failure of CP thin films.[11] Therefore, it is important to distinguish between the intermolecular forces that must be overcome to allow for reorganization of chains. Van der Waals interactions between the alkyl side chains of CPs are weaker and more easily overcome than interactions between rigid CP backbones,[16] which are considered load bearing.[4] The manifestation of this difference in strength on the ductility of CP materials is that backbone−backbone interactions inhibit reorganization of chains more than alkyl−alkyl interactions, which increases the likelihood of stress dissipation by chain pullout. Damage to the thin-film microstructure severs the electrical connection between polymer chains that necessarily span a thin film, leading to device degradation and ultimately failure.

To rationalize why mechanical differences exist between CP samples as a result of structural changes, it is important to gain insight into the conformation of these materials. Figure 1 illustrates two of the conformational factors, backbone linearity and twist (or conversely, coplanarity) between monomer units, which may vary between CP samples. CPs can be inhibited from reorganizing during deformation if their conjugated backbones are rigid, which is determined by the linearity of the conjugated backbone. CP chains that are less rigid have been shown to have a greater propensity to form kinks in their backbone, which increases their ductility because of entanglement.[17] The degree of coplanarity between monomer units in the backbone can also vary between polymer samples because of differences in the torsional potential energy curves between different bonds. Greater twist between monomer units can inhibit intermolecular interactions between polymer backbones but does not preclude chains from being linearly extended.

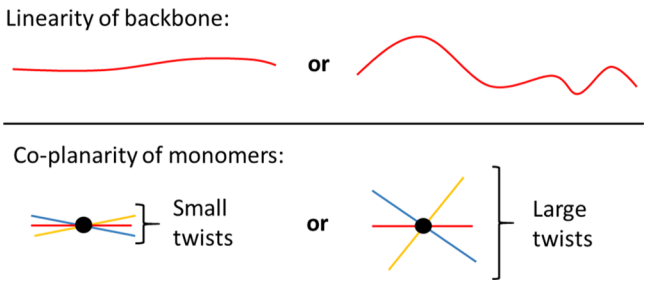

Figure 1. Topological drawings of polymer chains, shown in red, that are relatively linear and nonlinear (top). Drawings of trimers viewed down the long axis of the polymer backbone with different degrees of coplanarity between monomer units because of varying magnitudes (small or large) of twist between monomer units (bottom). Red, yellow, and blue lines represent the conjugated rings of separate monomers.

The solid-state structure of CP thin films also plays a role in determining the ability for polymer chains to deform. Characteristics of thin-film morphologies are affected by the size, shape, and distribution of solubilizing side chains attached to the polymer backbone.[18−20] For instance, it has been shown that introducing twist to polymer backbones decreases the number of interactions between polymer backbones during deformation, which leads to softer and more deformable materials.[21]

Crack onset strain (CoS) measurements provide a means to evaluate the ability for a polymer thin film to be extended before significant damage occurs. A polymer with a larger CoS displays a greater ability to be extended to larger strains before experiencing bulk failure.[22] In previous investigations, we had shown that two near-amorphous indacenodithiophene (IDT) copolymers, poly(indacenodithiophene-benzothiadiazole) (PIDTBT, frequently referred to as IDTBT) and poly(indacenodithiophene-benzopyrollodione) (PIDTBPD), display markedly different mechanical properties while maintaining good charge mobility.[23] Specifically, the CoS of PIDTBT and PIDTBPD was found to be 7 and >75%, respectively, despite having only marginal differences in their crystallinity profile.[23] Without differences in the crystalline volume fraction to point to as the reason for major differences in the CoS between these materials, the difference between PIDTBT and PIDTBPD is likely resultant from variations in other factors, such as differences in polymer backbone conformation and the overall solid-state structure that alter the material's ductility. Synthesis of random copolymers with varying amounts of the BPD monomer can allow us to ascribe changes in conformation because of gradual BPD incorporation to other factors that determine the material properties of CP thin films, which ultimately govern the hole mobility and CoS.

In this work, we synthesized a series of random IDT copolymers by varying the amount of benzothiadiazole (BT) and benzopyrollodione (BPD) comonomers. The incorporation was varied from 0 to 100% BPD content. This has allowed for a better understanding of why PIDTBT and PIDTBPD have markedly different material properties. As a result of BPD incorporation, the colinearity of the polymers remains unchanged but the hexadecyl side chains are more circularly distributed surrounding the polymer backbone in comparison to the side chains of PIDTBT which are extended in specific directions. Our results indicate that the change in ductility in these IDT-containing polymers is likely not due to changes in polymer backbone rigidity but is instead resultant from alterations in local side-chain distribution which is made more circular as the BPD monomer is incorporated.

RESULTS AND DISCUSSION

Direct arylation polymerization was performed to synthesize a series of random IDT copolymers (Scheme 1). By varying the feed ratios of comonomers BT and BPD while maintaining the IDT content (Table S1), we synthesized several polymers with IDT−comonomer distributions ranging from PIDTBT (no BPD comonomer) to PIDTBPD (only BPD comonomer). Incorporation of each monomer in the final polymer was assessed by ^{1}H NMR analysis (Table S5). Each random copolymer was named based on its BPD incorporation ratio; as such, the investigated polymer samples were named PIDTBT, 10% BPD, 35% BPD, 50% BPD, 75% BPD, 95% BPD, and PIDTBPD. Each polymer sample was analyzed by size exclusion chromatography (SEC) to evaluate its number average molecular weight (M_n) and dispersity ($Đ$). The results of this analysis are shown in Table 1.

https://dx.doi.org/10.1021/acs.macromol.0c00512
Macromolecules 2020, 53, 7511−7518

Scheme 1. Structure of Monomers and Resultant Random IDT Copolymers

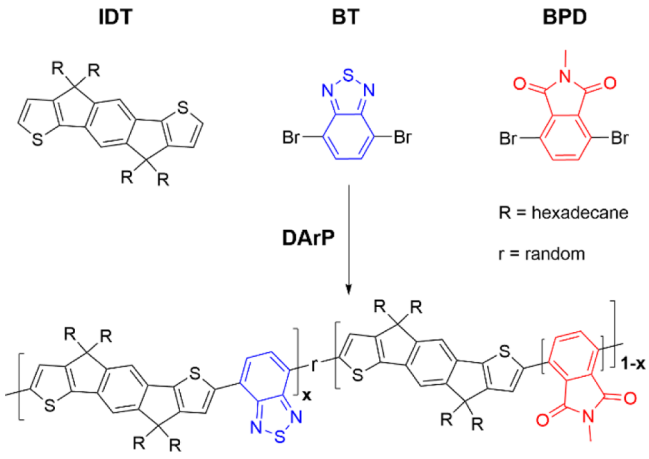

Table 1. BPD Incorporation Amount and SEC Data for Each Synthesized IDT Copolymer

BPD by ^{1}H NMR (%)	M_n (kg/mol)	$Đ$ (M_w/M_n)
0	9	1.6
10	10	1.7
35	11	1.6
50	14	1.8
75	18	1.8
95	18	2
100	29	1.8

With the polymers synthesized and monomer incorporation ratios and molecular size information having been established, we began to characterize the properties of each IDT copolymer, beginning with its optoelectronic properties. To do so, the polymers were subjected to ultraviolet−visible light absorption (UV−vis) and photoluminescence (PL) spectroscopy. Experiments were performed on both dilute solutions and spin-coated thin films, using chloroform as the solvent in both cases. Shown in Figure 2 are the thin-film UV−vis and PL spectra of all copolymers. In agreement with our previous studies,[23] the PIDTBT homopolymer displays an absorbance profile at much higher wavelengths than PIDTBPD because of its coplanar conjugated backbone. In both the PIDTBT and 10% BPD samples, a vibronic transition is readily apparent. Only one transition is observed in the solution spectra of any sample (Figure S2). The red-shifted peak at 670 nm is likely the 0−0 transition resultant from highly planar PIDTBT chains that, due to aggregation, display greater J-type behavior in their absorption profiles.[24] Only one transition is observed for the 35% BPD sample and beyond. J-type aggregation behavior and effective conjugation length of the polymer can be reduced when polymer backbone planarity is reduced. Thus, the observance of only one peak for the greater than 35% BPD samples could be due to the incorporation of BPD which could generate a twist between monomer units. The backbone twist is discussed later in the paper. The PL of the polymer systems gradually blue-shift as BPD is incorporated. The blue shift between the 95% BPD sample and PIDTBPD, in contrast, is much larger than the blue shifts between random copolymers. PIDTBPD, having no BT monomer, emits at a much smaller wavelength than any sample with BT. This may be derived from favorable delocalization of excitons to BT monomers on the polymer chain, which causes emission to occur from that position most frequently. The blue shift of the PL maximum for the random copolymers may be caused by shifts in BT energy levels as a result of having neighboring BPD units in the polymer chains.

Grazing incidence wide-angle X-ray scattering (GIWAXS) was performed to probe the crystallite d-spacings, crystallite orientations, and crystallite coherence lengths of each copolymer. The raw 2D GIWAXS spectra are shown in Figure S3. Although all samples are near-amorphous in terms of their overall solid-state structure, there are observable differences between the crystallographic features arising from these low-crystallinity materials. By observing these differences and rationalizing why they occur, inferences can be drawn about the conformational properties of each polymer sample. All (co)polymers show a mixture of face-on and edge-on orientation of polymer crystallites, evident by the appearance of both the side-chain (h00) and $\pi-\pi$ diffraction peaks (010) in the out-of-plane direction. The (h00) and (010) peaks in all samples appear diffuse and broad, suggesting the highly disordered, amorphous-like nature of the polymers under investigation (Figure S3). The thickness-normalized diffraction intensity of the (010) signal (extracted from vertical linecuts), which arises from $\pi-\pi$ stacking between polymer backbones, remains effectively constant throughout the spectrum (Figure S5). The $\pi-\pi$ d-spacing between the crystallites rises steadily with BPD incorporation from 35% BPD onward; from about 0.41 to 0.44 nm for 70% BPD and PIDTBPD, respectively (Figure 3a). The 0.41 nm (010) d-spacing distance has been observed for PIDTBT previously.[9] Notably, in samples with high BT content, we observe a characteristic rod-like diffraction peak (001) near $q \sim 0.4$ A^{-1} corresponding to diffraction from the polymer backbone. The (001) peaks are observed predominantly in the in-plane direction, indicating the highly in-plane orientation of the polymer backbone for all samples. Upon increasing BPD content, there is also a steady decline of both the intensity and coherence length of the (001) signal (Figure 3b,c). The (001) signal is the along-backbone diffraction and arises when conjugated chain segments are coplanar,[25] either by their intrinsic conformational properties

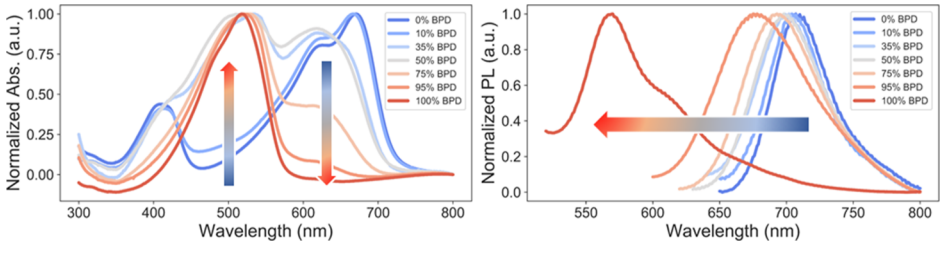

Figure 2. Thin-film (a) UV−vis absorbance and (b) PL data of all IDT copolymers.

https://dx.doi.org/10.1021/acs.macromol.0c00512
Macromolecules 2020, 53, 7511−7518

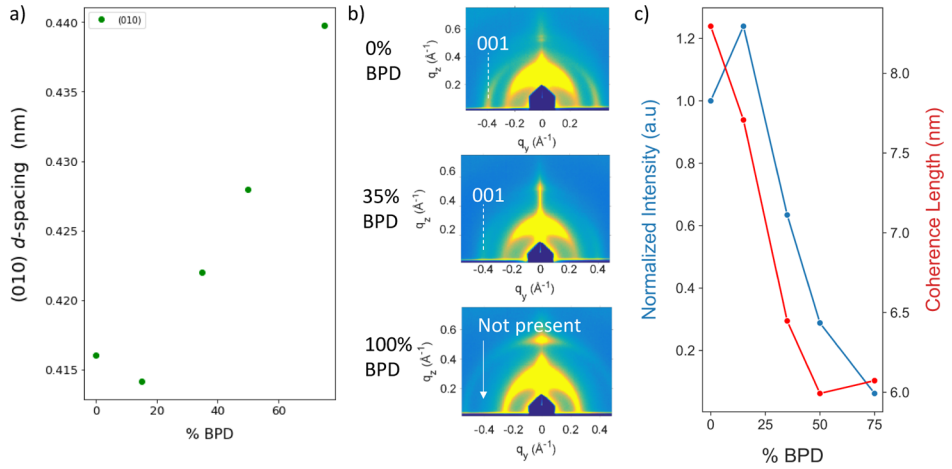

Figure 3. (a) (010) *d*-spacings, (b) zoomed-in regions of the raw-GIWAXS data, and (c) the normalized intensity and coherence length of the (001) backbone reflection signal.

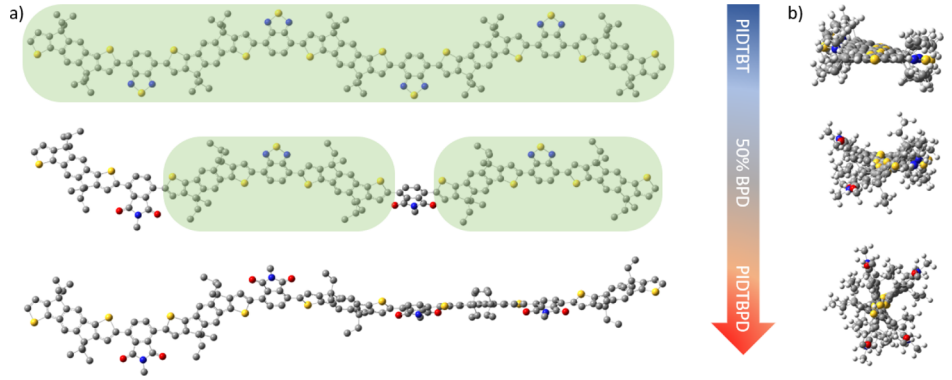

Figure 4. Density functional theory calculations of PIDTBT, 50% BPD, and PIDTBPD 9-mer optimized geometries from two perspectives: (a) from above the polymer backbone and (b) through the long axis of the polymer backbone.

or through induced coplanarity because of aggregation with other chains.[26] This signal has been observed for rigid polymers, including PIDTBT, and has been shown to disappear because of increased twist between monomer units in the backbone.[27] The first significant change in intensity and coherence length of this peak relative to PIDTBT occurs at 35% BPD incorporation. The signal is greatly diminished in the 50% BPD sample and continues to decrease as BPD is further incorporated. The observed changes in both the (010) and (001) signals, as a result of BPD incorporation, signify that by increasing the twisting between monomer units along the polymer backbone, there is more space between them and that polymer chains become less coplanar.

With knowledge that BPD incorporation alters the microstructure of these IDT copolymer systems, the structures of three IDT copolymers were simulated to elucidate how incorporation of the BPD monomer would impact the conformations of polymer chains. Each polymer was modeled to have five IDT repeat units and a total of four BT and/or BPD units, as shown in Figure 4a. The hexadecyl side chains on IDT have been replaced with ethyl groups, which are sufficiently long to accurately simulate the torsional potentials between monomers.[28] The chains in Figure 4 are in the favored all-anti configuration and as such will be the most linearly extended form of the polymer as the net direction of backbone deflection angles sum to zero.[29] Density functional theory (DFT) simulations suggest that this is appropriate as analysis of the potential energy of the torsional potential wells of each bond show that both polymers have a large preference for their anti-configuration (Figure S7). As a result, the low M_n chains are anticipated to display only anti-linkages, be linearly extended and not entangled, and therefore be rigid (Table S2).[28,29] Based on these results, we propose that the difference in CoS between PIDTBT, PIDTBPD, and of the random copolymers should not be attributed to differences in backbone rigidity and thus entanglement, despite their differences in M_n.

There is a larger dihedral angle between IDT−BPD linkages compared to IDT−BT, which imparts a twist to the polymer backbone. The impact of induced change is evident in the 50% BPD 9-mer with two BT and two BPD comonomers and is further exacerbated in PIDTBPD which twists more aggressively. Although repeat units of IDT−BT−IDT (Figure 4a, highlighted in green) remain planar in the simulated 50% BPD sample, BPD monomer units interrupt this planarity between the conjugated rings and twist the planar segments out of plane from each other. This is proposed to be the reason behind the reduction in the (100) crystallographic signal intensity and coherence length. Because of increased twist along the backbone, charge transport will weaken,[30] unless the planar segments that do exist provide enough regions of sufficient planarity for long-range transport along the backbone, bolstering the mobility despite this conformational change. The planar segments may also provide locations for favorable interactions between where strong electronic

https://dx.doi.org/10.1021/acs.macromol.0c00512
Macromolecules 2020, 53, 7511−7518

coupling between chains may form, giving rise to intermolecular charge transport.[31]

Twist between IDT−BPD monomers along the polymer backbone also alters the circular profile by which side chains extend away from the polymer backbone. As can be viewed by looking down the long axis of the polymer backbone (Figure 4b), the side chains of PIDTBT extend in a more organized pattern compared to the side chains of PIDTBPD, where the side chains extend away from the backbone across a larger range of angles. These side chains form a cylindrical tube that extends over the length of the polymer backbone. Increased shielding of the polymer backbone by alkyl side chains has been shown to decrease the occurrence of interactions between stiff backbones, favoring instead interactions between alkyl side chains, of non-CPs.[16] Greater disorder in side-chain extension has been shown to increase the extensibility of thin films.[32] Incorporation of the BPD monomer and the resultant change in the side-chain extension profile may disrupt PIDTBPD's ability to exhibit interactions between polymer backbones during deformation,[19] relative to PIDTBT, thus improving the ductility of PIDTBPD thin films.

Fast scanning calorimetry (FSC) was performed to determine the thermal behavior of our polymer systems, focusing on the homopolymers PIDTBT and PIDTBPD, as it is known that important mechanical properties of polymers strongly depend on thermal transition temperatures such as glass transition temperature (T_g) and melting temperatures (T_m).[33] The T_g values of fully vitrified PIDTBT and PIDTBPD were determined measuring the enthalpic relaxation overshoot of the amorphous phase of the films after physical aging (Figure 5).[34,35] Both polymers display a very comparable T_g (10 and 8 °C for PIDTBPD and PIDTBT, respectively). Accordingly, IDT copolymers comprising BPD moieties can be expected to have T_g's in the same temperature regime.

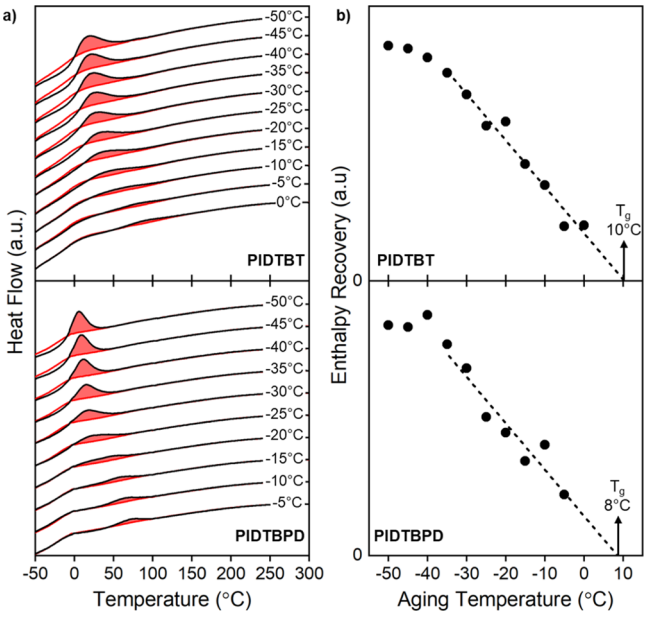

Figure 5. (a) FSC heating thermograms comparing aged (black) and unaged (red) PIDTBT (top panel) and PIDTBPD (bottom panel). Enthalpic overshoots (red highlighted areas) are observed when the aging temperatures (indicated on the right of the graph) were below the glass transition temperature of the materials. (b) Extrapolating the enthalpy recovery between aged and unaged samples of PIDTBT (top panel) and PIDTBPD (bottom panel) allows for determination of the temperature at which the enthalpy overshoot is zero. This temperature correlates to the onset of the glass transition temperature.

Considering their T_g's, these materials would be expected to soften at room temperature. However, it is important to note that two distinct endotherms appear when annealing the polymers above their T_g's (rather than aging below T_g; Figure S9). The presence of these enthalpic overshoots (compared to pristine samples) suggests possible liquid-crystalline or liquid-crystalline-like transitions, assisted by side-chain softening. Indeed, the lower temperature endotherms are reminiscent of sub-T_g transitions of CPs attributed to side-chain motion.[36,37] This process seems to occur at temperatures notably below room temperature (around 0 °C) for PIDTBPD, while for PIDTBT, the transition is around room temperature with a tail reaching 100 °C, not unlikely to affect their mechanical behavior. The investigation of the physical origin of the observed thermal transitions is a subject of future study.

To evaluate how incremental substitution of the BPD unit impacts electrical properties, OFETs were fabricated using each polymer system as the transport layer. The detailed results of OFET characterization are shown in Tables S3 and S4, and several sample transfer curves are shown in Figure S8. As can be seen in Figure 6 in blue, the hole mobility

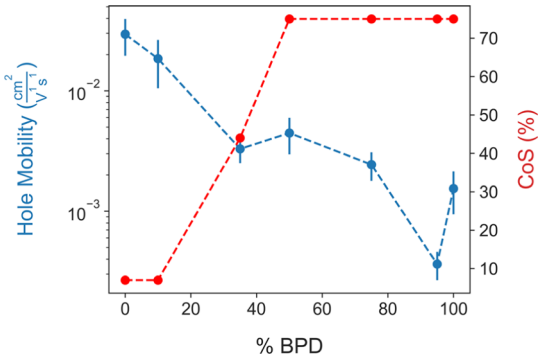

Figure 6. Hole mobility data from OFET measurements (blue) and CoS (red) vs % BPD of each IDT copolymer. The 50% BPD, 75% BPD, 90% BPD, and PIDTBPD samples were each extended to the limit of our strain stage (75% strain) without observed cracking.

immediately decreases with 10% BPD incorporation, followed by a decline to nearly that of PIDTBPD at a level of only 35% BPD incorporation. The 95% BPD sample has a lower mobility than that of PIDTBPD. This is likely caused by the small amount of BT monomer contributing little in the way of planarizing the molecule and only detrimentally acting like a structural defect. We ascribe the immediate decline in mobility to the increased twist between monomer units which weakens the electronic coupling between adjacent conjugated rings, thereby decreasing the efficiency of intramolecular charge transport.[38] As the BPD monomer is further incorporated into the backbone, charge transport along the backbone worsens. The distance between $\pi-\pi$ interactions in local aggregates also lengthens, as evidenced by the increase in (010) d-spacing beginning at 35% BPD incorporated and beyond, making intermolecular charge transfers less efficient.[39] Both effects contribute to the rapid decline of hole mobility and stem directly from the impact of the large twist between IDT and BPD units. The 9-mer DFT structural optimizations suggest that planar IDT−BT−IDT repeat units would remain in

https://dx.doi.org/10.1021/acs.macromol.0c00512
Macromolecules 2020, 53, 7511−7518

random copolymers, but the magnitude of hole mobility for the 35% BPD sample and the fact that the normalized intensity of the (010) $\pi-\pi$ stacking signal is not significantly different across all samples, demonstrate that charges must be transported along coplanar chain segments of greater length, longer than those that exist in the 35% BPD samples, to retain the hole mobility of PIDTBT.

CoS testing was performed to evaluate the extensibility of thin films made using each polymer. The results are shown on the red curve of Figure 6. The 10% BPD sample has an equivalent CoS to that of PIDTBT, signifying that the ductility of the polymer sample is not as sensitive to random incorporation of BPD as the electronic properties are. The 35% BPD sample, however, displayed a larger CoS of 44%. Because analysis of the DFT simulations of torsional potentials suggests that the polymer chains are expected to be linearly extended and the initial change in CoS occurs between polymers of similar M_n, this rise is likely affected by the twist between monomer units alone, rather than a difference in linearity or M_n. This conformational change was shown to impact the profile by which alkyl side chains extend away from the polymer backbone, such that greater BPD incorporation leads to a more cylindrical coverage of the polymer backbone. The 50% BPD, 75% BPD, 90% BPD, and PIDTBPD samples were each extended to the limit of our strain stage (75% strain) without observed cracking. Because interactions between rigid backbones can inhibit reorganization, we predict that the greater shielding of polymer backbones with increased BPD incorporation, because of the resultant circular extension of alkyl side chains, allows them to deform by decreasing the interactions between neighboring polymer backbones. In other words, as these chains reorient because of strain, they are deflected from their neighbors before localizing stress between polymer backbones.[21] The polymer backbones of chains with more circular alkyl side-chain extension are thus more able to slide past each other during deformation. This contributes to a higher CoS, by weakening the overall intermolecular interactions and alleviating stress through chain flow rather than chain pullout.

CONCLUSIONS

BPD incorporation alters the conformational properties of IDT polymer chains by increasing the average twist angle between monomer units. Despite this, DFT calculations suggest that BPD incorporation does not impact the rigidity of the polymer backbone. The hole mobility of these random IDT copolymers was highly sensitive to introduced twist because of the decrease in intramolecular charge transport efficiency. The increased twist also leads to a more varied circular distribution of IDT hexadecyl side chains extending away from the backbone. As a result, the side chains surround the backbone to a greater extent for more BPD-rich samples than for PIDTBT. Interestingly, FSC experiments demonstrate that this conformational change does not significantly alter the T_g's of these materials. We suggest that increased shielding of the polymer backbone with alkyl side chains, as a result of increased twist between monomer units due to BPD incorporation, shields the rigid backbones from load-bearing interactions between polymer backbones which would otherwise inhibit chain reorganization and lead to chain pullout. This allows the polymer chains with more circular side-chain distribution to slide past each other more easily during elongation of the film, which increases their CoS. Also, FSC results suggest that other thermal transitions may play a role in differentiating the mechanical properties of IDT copolymers. These descriptions of possible deformation mechanisms require experimental confirmation, but we believe them to be important in understanding the links between conformational properties, thin film morphologies, and the mechanical properties of near-amorphous CPs and provide a pathway to design high charge mobility polymeric materials with increased ductility.

ASSOCIATED CONTENT

Supporting Information

The Supporting Information is available free of charge at https://pubs.acs.org/doi/10.1021/acs.macromol.0c00512.

Experimental details regarding polymer synthesis, DFT calculations, ^{1}H NMR characterization, SEC characterization, optoelectronic measurements, crystallographic measurements, charge transport property measurements, CoS measurements, supplemental figures and tables, and ^{1}H NMR spectra of all polymers (PDF)

AUTHOR INFORMATION

Corresponding Author

Christine K. Luscombe − *Department of Chemistry, Department of Materials Science and Engineering, and Molecular Engineering & Sciences Institute, University of Washington, Seattle, Washington 98195, United States;* orcid.org/0000-0001-7456-1343; Email: luscombe@uw.edu

Authors

Parker J. W. Sommerville − *Department of Chemistry, University of Washington, Seattle, Washington 98195, United States*

Yilin Li − *Department of Materials Science and Engineering, University of Washington, Seattle, Washington 98195, United States;* orcid.org/0000-0001-9408-6738

Ban Xuan Dong − *Pritzker School of Molecular Engineering, University of Chicago, Chicago, Illinois 60637, United States;* orcid.org/0000-0002-2873-5207

Yongcao Zhang − *Department of Materials Science and Engineering, University of Washington, Seattle, Washington 98195, United States*

Jonathan W. Onorato − *Department of Materials Science and Engineering, University of Washington, Seattle, Washington 98195, United States;* orcid.org/0000-0003-1349-8277

Wesley K. Tatum − *Department of Materials Science and Engineering, University of Washington, Seattle, Washington 98195, United States;* orcid.org/0000-0003-0395-6975

Alex H. Balzer − *School of Chemical & Biomolecular Engineering, Georgia Institute of Technology, Atlanta, Georgia 303332, United States*

Natalie Stingelin − *School of Chemical & Biomolecular Engineering and School of Materials Science & Engineering, Georgia Institute of Technology, Atlanta, Georgia 303332, United States*

Shrayesh N. Patel − *Pritzker School of Molecular Engineering, University of Chicago, Chicago, Illinois 60637, United States; Materials Science Division, Argonne National Laboratory, Lemont, Illinois 60439, United States;* orcid.org/0000-0003-3657-827X

Paul F. Nealey − *Pritzker School of Molecular Engineering, University of Chicago, Chicago, Illinois 60637, United States;*

https://dx.doi.org/10.1021/acs.macromol.0c00512
Macromolecules 2020, 53, 7511−7518

Chemical Science and Engineering Division, Argonne National Laboratory, Lemont, Illinois 60439, United States;
orcid.org/0000-0003-3889-142X

Complete contact information is available at:
https://pubs.acs.org/10.1021/acs.macromol.0c00512

Notes

The authors declare no competing financial interest.

■ ACKNOWLEDGMENTS

The work was supported in part by the U.S. Department of Energy (DOE), Office of Science, Basic Energy Sciences (BES), under award DE-SC0020046 (P.J.W.S.), NSF DMR-1922259 (J.W.O. and B.X.D.), NSF DMR-1708317 (W.K.T.), and under the CCI Center for Selective C−H Functionalization, CHE-1700982 (Y.L.). Part of this work was conducted at the UW Photonics Center and Research Training Testbeds supported by the Clean Energy Institute and the Molecular Analysis Facility, a National Nanotechnology Coordinated Infrastructure site at the University of Washington which is supported in part by the National Science Foundation (grant NNCI-1542101), the University of Washington, the Molecular Engineering & Sciences Institute, and the Clean Energy Institute. The DFT calculations were made possible using the advanced computational, storage, and networking infrastructure provided by the Hyak supercomputer system at the University of Washington. The GIWAXS measurement used resources of the Advanced Photon Source, a DOE Office of Science User Facility operated for the DOE Office of Science by Argonne National Laboratory under contract no. DE-AC02-06CH11357.

■ REFERENCES

(1) Sirringhaus, H. 25th Anniversary Article: Organic Field-Effect Transistors: The Path Beyond Amorphous Silicon. *Adv. Mater.* **2014**, *26*, 1319−1335.
(2) Li, G.; Chang, W.-H.; Yang, Y. Low-Bandgap Conjugated Polymers Enabling Solution-Processable Tandem Solar Cells. *Nat. Rev. Mater.* **2017**, *2*, 17043.
(3) Wang, G.-J. N.; Gasperini, A.; Bao, Z. Stretchable Polymer Semiconductors for Plastic Electronics. *Adv. Electron. Mater.* **2018**, *4*, 1700429.
(4) Root, S. E.; Savagatrup, S.; Printz, A. D.; Rodriquez, D.; Lipomi, D. J. Mechanical Properties of Organic Semiconductors for Stretchable, Highly Flexible, and Mechanically Robust Electronics. *Chem. Rev.* **2017**, *117*, 6467−6499.
(5) Woo, C. H.; Piliego, C.; Holcombe, T. W.; Toney, M. F.; Fréchet, J. M. J. A Quantitative Correlation between the Mobility and Crystallinity of Photo-Cross-Linkable P3HT. *Macromolecules* **2012**, *45*, 3057−3062.
(6) Joseph Kline, R.; DeLongchamp, D. M.; Fischer, D. A.; Lin, E. K.; Richter, L. J.; Chabinyc, M. L.; Toney, M. F.; Heeney, M.; McCulloch, I. Critical Role of Side-Chain Attachment Density on the Order and Device Performance of Polythiophenes. *Macromolecules* **2007**, *40*, 7960.
(7) Noriega, R.; Salleo, A.; Spakowitz, A. J. Chain Conformations Dictate Multiscale Charge Transport Phenomena in Disordered Semiconducting Polymers. *Proc. Natl. Acad. Sci. U.S.A.* **2013**, *110*, 16315−16320.
(8) Bronstein, H.; Leem, D. S.; Hamilton, R.; Woebkenberg, P.; King, S.; Zhang, W.; Ashraf, R. S.; Heeney, M.; Anthopoulos, T. D.; Mello, J. d.; McCulloch, I. Indacenodithiophene- Co -Benzothiadiazole Copolymers for High Performance Solar Cells or Transistors via Alkyl Chain Optimization. *Macromolecules* **2011**, *44*, 6649−6652.
(9) Zheng, Y.; Wang, G. J. N.; Kang, J.; Nikolka, M.; Wu, H. C.; Tran, H.; Zhang, S.; Yan, H.; Chen, H.; Yuen, P. Y.; Mun, J.; Dauskardt, R. H.; McCulloch, I.; Tok, J. B. H.; Gu, X.; Bao, Z. An Intrinsically Stretchable High-Performance Polymer Semiconductor with Low Crystallinity. *Adv. Funct. Mater.* **2019**, *29*, 1905340.
(10) Yao, Y.; Dong, H.; Hu, W. Charge Transport in Organic and Polymeric Semiconductors for Flexible and Stretchable Devices. *Adv. Mater.* **2016**, *28*, 4513−4523.
(11) Alkhadra, M. A.; Root, S. E.; Hilby, K. M.; Rodriquez, D.; Sugiyama, F.; Lipomi, D. J. Quantifying the Fracture Behavior of Brittle and Ductile Thin Films of Semiconducting Polymers. *Chem. Mater.* **2017**, *29*, 10139−10149.
(12) Savagatrup, S.; Makaram, A. S.; Burke, D. J.; Lipomi, D. J. Mechanical Properties of Conjugated Polymers and Polymer-Fullerene Composites as a Function of Molecular Structure. *Adv. Funct. Mater.* **2014**, *24*, 1169−1181.
(13) Wang, M.; Baek, P.; Akbarinejad, A.; Barker, D.; Travas-Sejdic, J. Conjugated Polymers and Composites for Stretchable Organic Electronics. *J. Mater. Chem. C* **2019**, *7*, 5534−5552.
(14) Onorato, J.; Pakhnyuk, V.; Luscombe, C. K. Structure and Design of Polymers for Durable, Stretchable Organic Electronics. *Polym. J.* **2017**, *49*, 41−60.
(15) Lin, B.; Taylor, P. L. Dynamics of Polymer Chain Pull-Out. *Macromolecules* **1994**, *27*, 4212−4219.
(16) Postema, A. R.; Liou, K.; Wudl, F.; Smith, P. Highly Oriented Low-Modulus Materials from Liquid-Crystalline Polymers: The Ultimate Penalty for Solubilizing Alkyl Side Chains. *Macromolecules* **1990**, *23*, 1842−1845.
(17) Root, S. E.; Jackson, N. E.; Savagatrup, S.; Arya, G.; Lipomi, D. J. Modelling the Morphology and Thermomechanical Behaviour of Low-Bandgap Conjugated Polymers and Bulk Heterojunction Films. *Energy Environ. Sci.* **2017**, *10*, 558−569.
(18) Lu, C.; Lee, W.-Y.; Gu, X.; Xu, J.; Chou, H.-H.; Yan, H.; Chiu, Y.-C.; He, M.; Matthews, J. R.; Niu, W.; Tok, J. B.-H.; Toney, M. F.; Chen, W.-C.; Bao, Z. Effects of Molecular Structure and Packing Order on the Stretchability of Semicrystalline Conjugated Poly(Tetrathienoacene-Diketopyrrolopyrrole) Polymers. *Adv. Electron. Mater.* **2017**, *3*, 1600311.
(19) Sugiyama, F.; Kleinschmidt, A. T.; Kayser, L. V.; Rodriquez, D.; Fin, M.; Alkhadra, M. A.; Wan, J. M.-H.; Ramírez, J.; Chiang, S.-C.; Root, S. E.; Savagatrup, S.; Lipomi, D. J. Effects of Flexibility and Branching of Side Chains on the Mechanical Properties of Low-Bandgap Conjugated Polymers. *Polym. Chem.* **2018**, *9*, 4354−4363.
(20) Cao, Z.; Galuska, L.; Qian, Z.; Zhang, S.; Huang, L.; Prine, N.; Li, T.; He, Y.; Hong, K.; Gu, X. The Effect of Side-Chain Branch Position on the Thermal Properties of Poly(3-Alkylthiophenes). *Polym. Chem.* **2020**, *11*, 517.
(21) Jin, Y.-J.; Bae, J.-E.; Cho, K.-S.; Lee, W.-E.; Hwang, D.-Y.; Kwak, G. Room Temperature Fluorescent Conjugated Polymer Gums. *Adv. Funct. Mater.* **2014**, *24*, 1928−1937.
(22) Balar, N.; O'Connor, B. T. Correlating Crack Onset Strain and Cohesive Fracture Energy in Polymer Semiconductor Films. *Macromolecules* **2017**, *50*, 8611−8618.
(23) Li, Y.; Tatum, W. K.; Onorato, J. W.; Zhang, Y.; Luscombe, C. K. Low Elastic Modulus and High Charge Mobility of Low-Crystallinity Indacenodithiophene-Based Semiconducting Polymers for Potential Applications in Stretchable Electronics. *Macromolecules* **2018**, *51*, 6352−6358.
(24) Eder, T.; Stangl, T.; Gmelch, M.; Remmerssen, K.; Laux, D.; Höger, S.; Lupton, J. M.; Vogelsang, J. Switching between H- and J-Type Electronic Coupling in Single Conjugated Polymer Aggregates. *Nat. Commun.* **2017**, *8*, 1641.
(25) Zhang, X.; Bronstein, H.; Kronemeijer, A. J.; Smith, J.; Kim, Y.; Kline, R. J.; Richter, L. J.; Anthopoulos, T. D.; Sirringhaus, H.; Song, K.; Heeney, M.; Zhang, W.; McCulloch, I.; DeLongchamp, D. M. Molecular Origin of High Field-Effect Mobility in an Indacenodithiophene−Benzothiadiazole Copolymer. *Nat. Commun.* **2013**, *4*, 2238.

(26) Wang, S.; Fabiano, S.; Himmelberger, S.; Puzinas, S.; Crispin, X.; Salleo, A.; Berggren, M. Experimental Evidence That Short-Range Intermolecular Aggregation Is Sufficient for Efficient Charge Transport in Conjugated Polymers. *Proc. Natl. Acad. Sci. U.S.A.* **2015**, *112*, 10599−10604.
(27) Steyrleuthner, R.; Di Pietro, R.; Collins, B. A.; Polzer, F.; Himmelberger, S.; Schubert, M.; Chen, Z.; Zhang, S.; Salleo, A.; Ade, H.; Facchetti, A.; Neher, D. The Role of Regioregularity, Crystallinity, and Chain Orientation on Electron Transport in a High-Mobility n-Type Copolymer. *J. Am. Chem. Soc.* **2014**, *136*, 4245−4256.
(28) Lin, J. B.; Jin, Y.; Lopez, S. A.; Druckerman, N.; Wheeler, S. E.; Houk, K. N. Torsional Barriers to Rotation and Planarization in Heterocyclic Oligomers of Value in Organic Electronics. *J. Chem. Theory Comput.* **2017**, *13*, 5624−5638.
(29) Vezie, M. S.; Few, S.; Meager, I.; Pieridou, G.; Dörling, B.; Ashraf, R. S.; Goñi, A. R.; Bronstein, H.; McCulloch, I.; Hayes, S. C.; Campoy-Quiles, M.; Nelson, J. Exploring the Origin of High Optical Absorption in Conjugated Polymers. *Nat. Mater.* **2016**, *15*, 746−753.
(30) Hultell, M.; Stafström, S. Impact of Ring Torsion on the Intrachain Mobility in Conjugated Polymers. *Phys. Rev. B: Condens. Matter Mater. Phys.* **2007**, *75*, 104304.
(31) Thomas, T. H.; Harkin, D. J.; Gillett, A. J.; Lemaur, V.; Nikolka, M.; Sadhanala, A.; Richter, J. M.; Armitage, J.; Chen, H.; McCulloch, I.; Menke, S. M.; Olivier, Y.; Beljonne, D.; Sirringhaus, H. Short Contacts between Chains Enhancing Luminescence Quantum Yields and Carrier Mobilities in Conjugated Copolymers. *Nat. Commun.* **2019**, *10*, 2614.
(32) Printz, A. D.; Savagatrup, S.; Burke, D. J.; Purdy, T. N.; Lipomi, D. J. Increased Elasticity of a Low-Bandgap Conjugated Copolymer by Random Segmentation for Mechanically Robust Solar Cells. *RSC Adv.* **2014**, *4*, 13635−13643.
(33) Sharma, A.; Pan, X.; Campbell, J. A.; Andersson, M. R.; Lewis, D. A. Unravelling the Thermomechanical Properties of Bulk Heterojunction Blends in Polymer Solar Cells. *Macromolecules* **2017**, *50*, 3347−3354.
(34) Schick, C.; Mathot, V. B. F. *Fast Scanning Calorimetry*; Springer, 2016.
(35) Martín, J.; Stingelin, N.; Cangialosi, D. Direct Calorimetric Observation of the Rigid Amorphous Fraction in a Semiconducting Polymer. *J. Phys. Chem. Lett.* **2018**, *9*, 990−995.
(36) Balar, N.; Siddika, S.; Kashani, S.; Peng, Z.; Rech, J. J.; Ye, L.; You, W.; Ade, H.; O'Connor, B. T. Role of Secondary Thermal Relaxations in Conjugated Polymer Film Toughness. *Chem. Mater.* **2020**, *32*, 6540−6549.
(37) Sharma, A.; Pan, X.; Bjuggren, J. M.; Gedefaw, D.; Xu, X.; Kroon, R.; Wang, E.; Campbell, J. A.; Lewis, D. A.; Andersson, M. R. Probing the Relationship between Molecular Structures, Thermal Transitions, and Morphology in Polymer Semiconductors Using a Woven Glass-Mesh-Based DMTA Technique. *Chem. Mater.* **2019**, *31*, 6740−6749.
(38) Meyer, D. L.; Schmidt-Meinzer, N.; Matt, C.; Rein, S.; Lombeck, F.; Sommer, M.; Biskup, T. Side-Chain Engineering of Conjugated Polymers: Distinguishing Its Impact on Film Morphology and Electronic Structure. *J. Phys. Chem. C* **2019**, *123*, 20071−20083.
(39) Son, S. Y.; Kim, Y.; Lee, J.; Lee, G.-Y.; Park, W.-T.; Noh, Y.-Y.; Park, C. E.; Park, T. High-Field-Effect Mobility of Low-Crystallinity Conjugated Polymers with Localized Aggregates. *J. Am. Chem. Soc.* **2016**, *138*, 8096−8103.

■ NOTE ADDED AFTER ASAP PUBLICATION

Due to a production error, the version of this paper that was published ASAP August 18, 2020, listed incorrect affiliations for two authors. The corrected version was reposted August 19, 2020.

https://dx.doi.org/10.1021/acs.macromol.0c00512
Macromolecules 2020, 53, 7511−7518